

Rational designing and crystal structure prediction of ring-fused double-PDI compounds as n-channel organic semiconductors: A DFT study

Suryakanti Debata, Smruti R. Sahoo, Rudranarayan Khatua, Sridhar Sahu

High Performance Computing lab, Department of Physics, Indian Institute of Technology
(Indian School of Mines) Dhanbad, India

Table S1. Comparison of the frontier molecular orbitals (FMOs) of DCPP-1, calculated at different density functional theory (DFT) levels using 6-311G(d,p) basis set, with the experimental values. (B3LYP: 20% HF, PBE0: 25% HF).

Compound	Method	HOMO (eV)	LUMO (eV)	E _g (eV)
DPDI-1	Expt.	-----	-3.90	-----
	B3LYP	-6.269	-3.858	2.411
	PBE0	-6.468	-3.796	2.672
	B3LYP-D3	-6.266	-3.858	2.408
	B3LYP-D3(BJ)	-6.265	-3.856	2.409

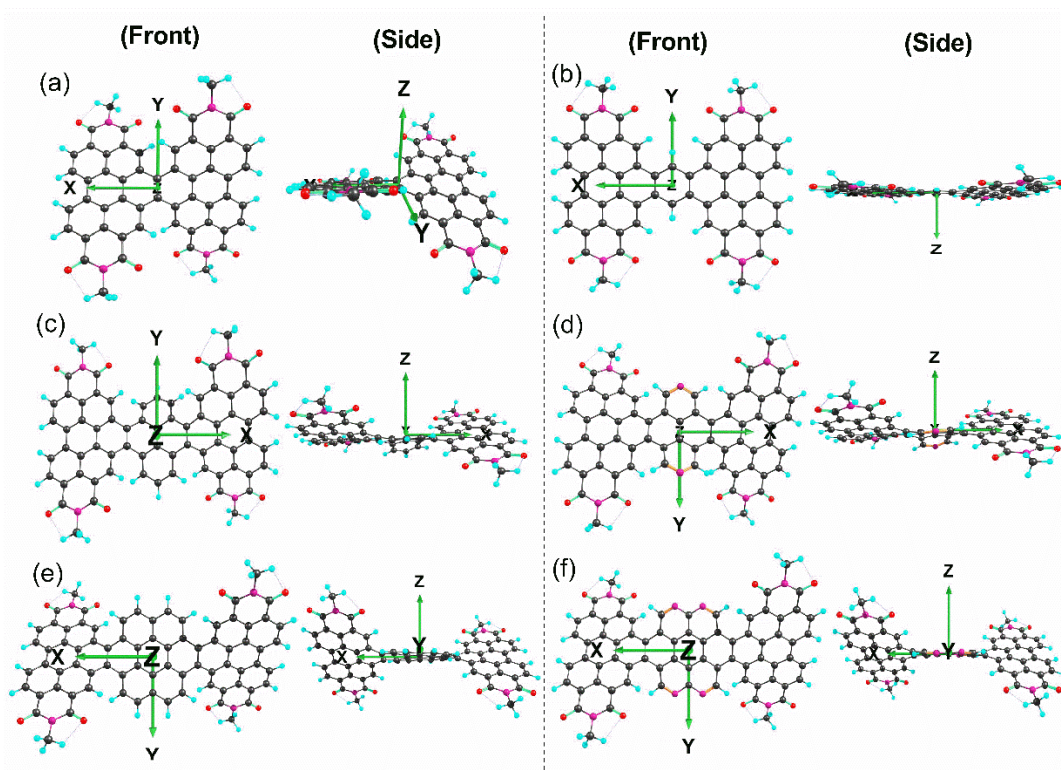


Figure S1. Orientation of the studied DPDI-molecules along the three axes: (a) DPDI-1, (b) DPDI-2, (c) DPDI-3, (d) DPDI-4, (e) DPDI-5 and (f) DPDI-6. Front and side views of the molecules are shown here for better visualization.

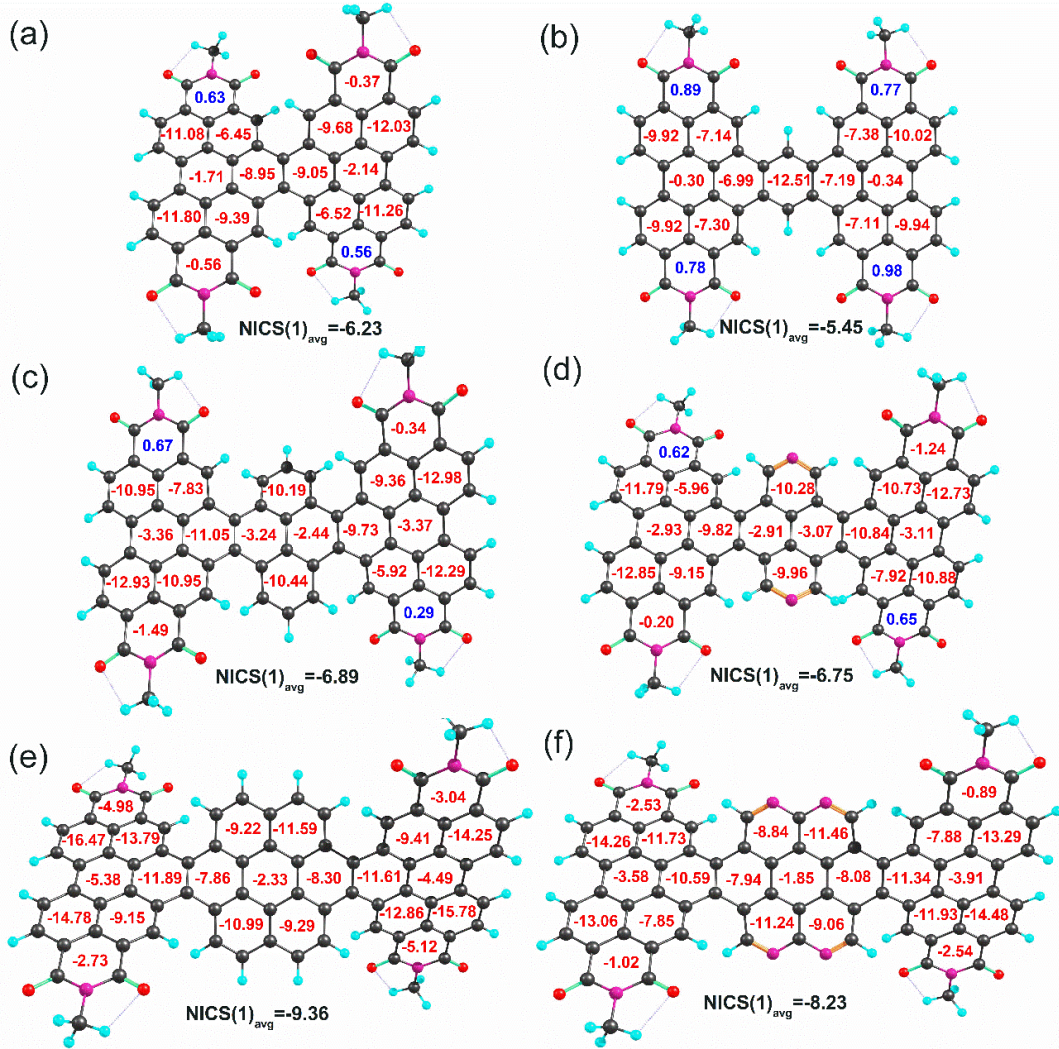


Figure S2. NICS(1) values of DPDI-compounds calculated at B3LYP/6-31+G(d,p) level, where the negative values correspond to the aromaticity of the ring and positive values correspond to antiaromaticity.

Table S2. Frontier molecular orbital (HOMO and LUMO) energies and HOMO-LUMO gaps of the DPDI-molecules.

Compound	Theoretical			Experimental
	HOMO (eV)	LUMO (eV)	HOMO-LUMO gap (ΔE) (eV)	LUMO (eV)
DPDI-1	-6.266	-3.858	2.408	-3.90 [S1]
DPDI-2	-6.098	-3.772	2.326	-4.04 [S2]
DPDI-3	-6.175	-3.573	2.602	-3.74 [S3]
DPDI-4	-6.379	-3.688	2.691	-----
DPDI-5	-5.914	-3.620	2.294	-----
DPDI-6	-6.439	-3.885	2.554	-----

Table S3. Molecular orbitals (HOMO and LUMO) of the DPDI molecules obtained at B3LYP-D3/6-311G(d,p) level of theory.

Compound	HOMO	LUMO
DPDI-1		
DPDI-2		
DPDI-3		
DPDI-4		
DPDI-5		
DPDI-6		

Section S1. Molecular electrostatic potential (ESP) surface analysis

The ESP profiles of the DPDI-compounds are presented in **Fig. S3**, where the intramolecular charge separation can be qualitatively visualized. In here, the red, green, and blue colors represent the electron-rich, neutral, and electron-deficient regions respectively. The increasing positive potential follows the order as represented in the color scale in the bottom. In all the molecules, the oxygen atoms are rich with electrons, whereas the benzene rings and hydrogen atoms accommodate positive charges. While comparing the effect of N-substitutions at the bridging positions of pyrene and coronene fused DPDI-compounds, we observed more negative charge on the bridges as compared to the undoped counterparts (DPDI-3 and 5). It may be resulting from the strong electron-withdrawing nature of N-atoms. This finding is in agreement with the lower LUMO levels of the N-doped DPDIs. Also, since the charge separation is significant in these compounds, it suggests their superior charge transport properties [S4, S5].

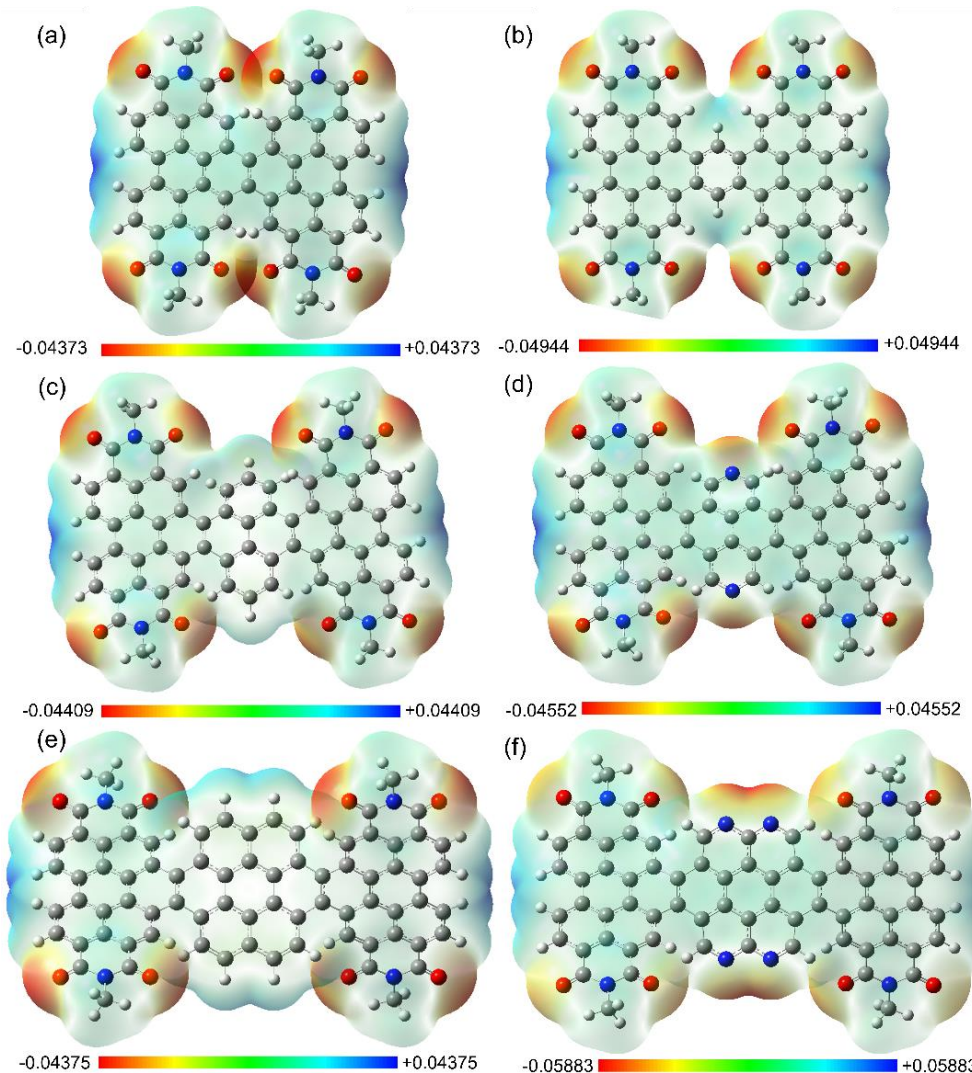


Figure S3. Molecular Electrostatic Potential (ESP) profiles of ring-fused DPDI-molecules. The red, green, and blue colors in the ESP surfaces represent the electron-rich, neutral, and electron-deficient regions respectively.

Section S2. Crystal structure prediction

Crystal structures of the DPDI-systems have been predicted through the Polymorph Predictor module of the Materials Studio package (17.1.0.48), using their optimized gas-phase conformations. In this calculation, the Polymorph Predictor quality was specified to a default fine setting, which anneals the sample in Monte Carlo simulation algorithm within a temperature range of 300.0 K to 100000.0 K, and a heating factor of 0.025. In this algorithm, the maximum number of steps is 7000, and 12 successive steps are accepted before cooling. Here, we have used the Dreiding forcefield in conjugation with Gasteiger charges. We restrict our calculation to the ten most common space groups of the organic compounds (P2₁/c, P1, P2₁2₁2₁, C2/c, P2₁, Pbca, Pna2₁, Pbcn, Cc, and C2), as registered in Cambridge Structural Database (CSD). The crystal structures have been sorted with respect to their total energies, and the lowest energy structure has been chosen for the further calculations [S6, S7].

Table S4. Space group and unit cell parameters of the DPDI-compounds calculated from the Polymorph Predictor module of the Materials Studio package.

Compound	Space group	Lattice parameters				
		a	b (Å)	c	α	β (°)
DPDI-1	Pna2 ₁	39.27	11.11	17.55	90.0	90.0
DPDI-2	Pna2 ₁	25.46	17.03	20.15	90.0	90.0
DPDI-3	Pna2 ₁	33.91	24.99	14.09	90.0	90.0
DPDI-4	P2 ₁ 2 ₁ 2 ₁	17.37	27.52	20.93	90.0	90.0
DPDI-5	Pna2 ₁	25.16	21.19	21.04	90.0	90.0
DPDI-6	P2 ₁ 2 ₁ 2 ₁	36.19	18.79	23.21	90.0	90.0

Table S5. Comparison of the as calculated μ_h/μ_e results with the several previously reported ring-fused PDIs.

Sl. No.	Compound	Experimental/ theoretical results	μ_h ($\text{cm}^2\text{V}^{-1}\text{s}^{-1}$)	μ_e ($\text{cm}^2\text{V}^{-1}\text{s}^{-1}$)	Ref.
1	PBDB-T:F2PDI-I	Experimental	2.14×10^{-4}	1.25×10^{-4}	[S8]
	PBDB-T:F2PDI-II		1.55×10^{-4}	7.6×10^{-4}	
2	PTB7-Th:DTC-PDI	Experimental	1.28×10^{-4}	2.19×10^{-5}	[S9]
	PTB7-Th: FDTC-PDI		6.49×10^{-4}	1.66×10^{-4}	
3	FT-FPDI	Experimental	4.93×10^{-4}	2.33×10^{-4}	[S10]
	FTT-FPDI		5.67×10^{-4}	4.11×10^{-4}	
4	Thieno-pyrido-thieno-isoquinoline-dione fused PDIs:	Experimental			
	Compound-2		2.0×10^{-4}	7.2×10^{-6}	
	Compound-3		8.5×10^{-4}	3.9×10^{-6}	[S11]
5	PTB7-Th:FPDI-F	Experimental	6.83×10^{-4}	3.17×10^{-7}	[S12]
	PTB7-Th:FPDI-T		6.71×10^{-3}	1.05×10^{-4}	
	PTB7-Th:FPDI-Se		2.59×10^{-3}	4.50×10^{-5}	
6	QU-PDI:PBDB-TFCI	Experimental	2.85×10^{-4}	4.41×10^{-4}	[S13]
7	PTB7-Th/BPDI-1	Experimental	1.06×10^{-4}	6.95×10^{-7}	[S14]
	PTB7-Th/BPDI-2		1.65×10^{-4}	7.29×10^{-7}	
8	CDT-PDI	Experimental	4.75×10^{-5}	3.10×10^{-5}	[S15]
	CDT-TFP		9.10×10^{-5}	1.25×10^{-4}	
	C8X- TFP		2.69×10^{-5}	1.34×10^{-4}	
9	PTB7-Th:BT-FPDI	Experimental	6.4×10^{-4}	4.3×10^{-4}	[S16]
10	DPDI-5	Theoretical	5.75×10^{-2}	1.62×10^{-2}	This work
	DPDI-6		4.75×10^{-2}	5.31×10^{-2}	

Table S6. The details of absorption wavelengths (λ_{abs}), oscillator strengths (f), excitation energies, and major compositions of DPDI-compounds. The excited-state transitions are calculated by TD-DFT method using CAM-B3LYP/6-311G(d,p) level of theory.

Compound	states	λ_{abs} (nm)	f	energy (eV)	composition
DPDI-1	S ₁	467.4	0.649	2.65	HOMO→LUMO (90%)
	S ₂	429.3	0.302	2.89	H-2→LUMO (81%), HOMO→L+2 (11%)
	S ₃	419.6	0.155	2.95	H-1→LUMO (53%), HOMO→L+1 (45%)
	S ₇	327.3	1.320	3.79	H-2→LUMO (13%), HOMO→L+2 (79%)
	S ₁₆	291.9	0.562	4.25	H-2→L+2 (74%), HOMO→L+7 (12%)
DPDI-2	S ₁	476.5	0.725	2.60	H-1→L+1 (10%), HOMO→LUMO (87%)
	S ₃	392.2	0.342	3.16	H-2→LUMO (73%), HOMO→L+2 (13%)
	S ₆	350.2	0.479	3.54	H-3→LUMO (27%), H-1→L+1 (61%)
	S ₈	315.8	2.205	3.93	H-2→LUMO (14%), HOMO→L+2 (71%)
DPDI-3	S ₁	442.2	0.549	2.80	H-3→L+1 (12%), HOMO→LUMO (70%)
	S ₂	429.1	0.676	2.89	H-2→L+1 (32%), H-1→LUMO (44%), H-1→L+1 (14%)
	S ₅	340.9	0.623	3.64	H-4→LUMO (16%), H-2→L+1 (13%), H-1→L+2 (16%), HOMO→L+2 (28%)
	S ₆	335.0	0.748	3.58	H-1→L+2 (36%), HOMO→L+2 (10%)
DPDI-4	S ₁	433.5	0.616	2.77	H-3→L+1 (12%), HOMO→LUMO (73%)
	S ₂	424.5	0.665	2.83	H-2→L+1 (29%), H-1→LUMO (45%), H-1→L+1 (10%)
	S ₅	336.7	0.710	3.56	H-3→L+1 (10%), H-1→L+2 (13%), HOMO→L+2 (31%), HOMO→L+3 (11%)
	S ₆	332.5	0.625	3.61	H-1→L+2 (13%), HOMO→L+2 (43%)
DPDI-5	S ₁	468.8	0.405	2.56	H-2→L+1 (16%), HOMO→LUMO (76%)
	S ₂	455.4	0.657	2.63	H-4→L+1 (11%), H-1→LUMO (73%)
	S ₇	372.8	1.336	3.22	H-1→L+3 (12%), HOMO→L+2 (62%)
	S ₉	335.6	1.098	3.58	H-4→L+1 (18%), H-2→L+4 (12%), H-1→L+3 (25%), HOMO→L+2 (14%)
DPDI-6	S ₁	450.8	0.999	2.66	H-1→LUMO (77%)
	S ₂	442.0	0.627	2.71	H-2→L+1 (31%), HOMO→LUMO (61%)
	S ₃	434.8	0.292	2.76	H-2→LUMO (51%), HOMO→L+1 (43%)
	S ₈	336.3	2.078	3.57	H-2→L+4 (12%), HOMO→L+3 (61%)

Section S3. Non-linear optical analysis

The non-linear optical response of the organic semiconductors can be estimated by the equation;

$$\mu_i = \mu_i^0 + \sum_j \alpha_{ij} F_j + \sum_{j,k} \frac{1}{2} \beta_{ijk} F_j F_k + \sum_{j,k,l} \frac{1}{6} \gamma_{ijkl} F_j F_k F_l + \dots \quad [8]$$

Where, μ_i and μ_i^0 represent the dipole moment of the i^{th} molecule with and without the applied electric field F . The symbols α_{ij} , β_{ijk} and γ_{ijkl} are the polarizability, first hyperpolarizability tensor and second hyperpolarizability tensor of the system respectively, which are the derivatives of the energy of the molecules with respect to the applied electric field. The indices i , j and k represent the cartesian coordinates [S17, S18].

The dipole moment (μ), mean static polarizability (α), polarizability anisotropy ($\Delta\alpha$) and the first order hyperpolarizability (β) of the compounds are the important parameters to study the NLO response of the system, which can be expressed as;

$$\mu = (\mu_x^2 + \mu_y^2 + \mu_z^2) \quad [9]$$

$$\alpha = \frac{1}{3} [\alpha_{xx} + \alpha_{yy} + \alpha_{zz}] \quad [10]$$

$$\Delta\alpha = \frac{1}{2} [(\alpha_{xx} - \alpha_{yy})^2 + (\alpha_{xx} - \alpha_{zz})^2 + (\alpha_{yy} - \alpha_{zz})^2 + 6(\alpha_{xy}^2 + \alpha_{xz}^2 + \alpha_{yz}^2)]^{\frac{1}{2}} \quad [11]$$

$$\beta_0 = [\beta_x^2 + \beta_y^2 + \beta_z^2]^{\frac{1}{2}} \quad [12]$$

Where, $\beta_x = \beta_{xxx} + \beta_{xxy} + \beta_{xzz}$, $\beta_y = \beta_{yyy} + \beta_{yzz} + \beta_{yxz}$, and $\beta_z = \beta_{zzz} + \beta_{zxx} + \beta_{zyy}$; also, we consider $\beta_{xxy} = \beta_{yxy} = \beta_{yyx}$, $\beta_{zyy} = \beta_{yzy} = \beta_{yyz}$, and so on, according to Kleinman symmetry.

Table S7. Components of dipole moment (μ) and static hyperpolarizability (β) projected along x-, y- and z-directions, calculated at CAM-B3LYP/6-311G(d,p) level of theory.

Compound	μ_x (a.u.)	μ_y (a.u.)	μ_z (a.u.)	β_x (a.u.)	β_y (a.u.)	β_z (a.u.)
DPDI-1	-9.75×10^{-3}	-1.84×10^{-3}	-1.63×10^{-2}	-7.99	-1.87	9.69
DPDI-2	-8.56×10^{-3}	1.51×10^{-3}	-1.66×10^{-3}	-7.31	-0.91	0.08
DPDI-3	-4.56×10^{-2}	-1.54×10^{-1}	-5.08×10^{-1}	600.51	280.31	1277.81
DPDI-4	-3.42×10^{-2}	-5.49×10^{-2}	-5.19×10^{-2}	326.89	292.63	823.46
DPDI-5	-5.00×10^{-5}	-4.61×10^{-3}	-1.26×10^{-5}	1.72	-5.99	0.01
DPDI-6	1.57×10^{-5}	3.88×10^{-3}	-4.33×10^{-5}	-0.25	5.19	0.08

Table S8. NLO Properties of DPDI-compounds: dipole moment (μ in Debye), polarizability (α in esu), and static/frequency dependent hyperpolarizabilities ($\beta(0,0,0)$, $\beta(-\omega,\omega,0)$, $\beta(-2\omega,\omega,0)$ in esu) calculated at CAM-B3LYP/6-311G(d,p) level.

Compound	μ (Debye)	α ($\times 10^{-24}$) (esu)	$\Delta\alpha$ ($\times 10^{-24}$) (esu)	$\beta(0,0,0)$ ($\times 10^{-30}$) (esu)	$\beta(-\omega,\omega,0)$ ($\times 10^{-30}$) (esu)	$\beta(-2\omega,\omega,0)$ ($\times 10^{-30}$) (esu)	Ref.
DPDI-1	0.048	116.638	101.638	0.110	0.123	0.238	
DPDI-2	0.022	127.325	137.867	0.064	0.054	0.125	
DPDI-3	1.355	147.265	134.360	12.429	15.745	27.971	This work
DPDI-4	0.211	145.256	136.121	8.056	9.995	16.587	
DPDI-5	0.012	172.688	144.738	0.054	0.043	0.100	
DPDI-6	0.009	168.151	154.483	0.044	0.040	0.019	
Urea	4.24	----	----	0.37	----	----	[S19]
Resorufin	20.602	25.117	----	12.477	----	----	[S20]
BDP-IMD dye	4.66- 5.63	50.6- 61.5	42476.4- 55454.9	42.4- 71.7	----	----	[S21]
Rigid coumarins	3.45- 6.78	56.67- 77.51	5161.27- 7963.07	11.94- 35.85	----	----	[S22]

(BDP-IMD: 2-benzimidazole-4,4-difluoro-4-bora-3a, 4a-diaza-s-indacene)

Here, 1 a. u. = 0.008629×10^{-30} esu, for first hyperpolarizability (β_0);

1 a. u. = 0.1482×10^{-24} esu, for static polarizability (α), polarizability anisotropy ($\Delta\alpha$) [S19].

References:

- S1. G. Gao, N. Liang, H. Geng, W. Jiang, H. Fu, J. Feng, J. Hou, X. Feng, Z. Wang, *J. Am. Chem. Soc.* 2017, 139, 15914-15920.
- S2. P. E. Hartnett, H. S. S. R. Matte, N. D. Eastham, N. E. Jackson, Y. Wu, L. X. Chen, M. A. Ratner, R. P. H. Chang, M. C. Hersam, M. R. Wasielewski, T. J. Marks, *Chem. Sci.*, 2016, 7, 3543-3555.
- S3. S. Liu, C. Li, Y. Xu, Z. Li, H. Huang, N. Fu, J. Shao, B. Zhao, H. Huang, W. Huang, *Dyes Pigm.*, 2020, 173, 107976.
- S4. S. Ahmed, B. C. Mushahary, D. J. Kalita, *ACS Omega*, 2020, 5, 8321–8333.
- S5. J. Deng, W. Hu, W. Shen, M. Li, R. He, *Phys. Chem. Chem. Phys.*, 2019, 21, 1235-1241.
- S6. H. Li, B. K. Bahuleyan, R. P. Johnson, Y. A. Shchipunov, H. Suh, C. -S. Ha, I. Kim, *J. Mater. Chem.*, 2011, 21, 17938-17945.
- S7. D. Alberga, I. Ciofini, G. F. Mangiatordi, A. Pedone, G. Lattanzi, J. Roncali, C. Adamo, *Chem. Mater.* 2017, 29, 673–681.
- S8. H. Wang, M. Li, J. Song, C. Li, Z. Bo, *Dyes Pigm.*, 2020, 183, 108736.
- S9. Z. Li, J. Wang, H. Huang, Y. Liu, Y. Yun, Z. Cheng, S. Liu, Z. Ding, B. Zhao, W. Huang, *New J. Chem.*, 2019, 43, 13775-13782.

- S10. Y. Yin, W. Zhang, Z. Zheng, Z. Ge, Y. Liu, F. Guo, S. Gao, L. Zhao, Y. Zhang, *J. Mater. Chem. C*, 2020, 8, 12516-12526.
- S11. B. Carlotti, Z. Cai, H. Kim, V. Sharapov, I. K. Madu, D. Zhao, W. Chen, P. M. Zimmerman, L. Yu, T. Goodson, *Chem. Mater.* 2018, 30, 4263-4276.
- S12. H. Zhong, C. -H. Wu, C. -Z. Li, J. Carpenter, C. -C. Chueh, J. -Y. Chen, H. Ade, A. K.-Y. Jen, *Adv. Mater.*, 2016, 28, 951-958.
- S13. J. Han, W. Shi, X. Wang, J. Cai, X. Hao, J. Shi, X. Bao, R. Yang, *J. Mater. Chem. A*, 2020, 8, 3918-3932.
- S14. X. Li, K. Wu, L. Zheng, Y. Deng, S. Tan, H. Chen, *Dyes Pigm.*, 2019, 168, 59-67.
- S15. J. Liu, H. Lu, Y. Liu, J. Zhang, C. Li, X. Xu, Z. Bo, *ACS Appl. Mater. Interfaces* 2020, 12, 10746–10754.
- S16. Y. Yin, Z. Zheng, D. Chen, M. Liu, J. Zhang, F. Guo, S. Gao, L. Zhao, Y. Zhang, *J. Mater. Chem. A*, 2019, 7, 27493-27502.
- S17. N. Matsuzawa, J. Seto, D. A. Dixon, *J. Phys. Chem. A*, 1997, 101, 9391–9398.
- S18. A. I. Daud, W. M. Khairul, E. Augustine, S. Arshad, I. A. Razak, *J. Mol. Struct.*, 2019, 1194, 124-137.
- S19. A. Irfan, A. G. Al-Sehemi, A. R. Chaudhry, S. Muhammad, A. M. Asiri, *Optik*, 2016, 127, 10148–10157.
- S20. M. J. K. Kuniyil, R. Padmanaban, *New J. Chem.*, 2019, 43, 13616.
- S21. S. S. Thakare, M. C. Sreenath, S. Chitrambalam, I. H. Joe, N. Sekar, *Opt. Mater.*, 2017, 64, 453-460.
- S22. S. K. Lanke, N. Sekar, *J Fluoresc.*, 2015, 25, 1469-1480.